

DETECTION OF PROMINENT STELLAR DISKS IN THE PROGENITORS OF PRESENT-DAY MASSIVE ELLIPTICAL GALAXIES

ROOZBEH H. DAVARI^{1,2}, LUIS C. HO^{3,4}, BAHRAM MOBASHER¹, AND GABRIELA CANALIZO¹

Accepted for published in The Astrophysical Journal

ABSTRACT

Massive galaxies at higher redshifts ($z > 2$) show different characteristics from their local counterparts: They are compact and most likely have a disk. In this study, we trace the evolution of local massive galaxies by performing a detailed morphological analysis, namely, fitting single Sérsic profiles and performing bulge+disk decompositions. We analyze ~ 250 massive galaxies selected from all CANDELS fields (COSMOS, UDS, EGS, GOODS-South and GOODS-North). We confirm that both star-forming and quiescent galaxies increase their sizes significantly from $z \approx 2.5$ to the present day. The global Sérsic index of quiescent galaxies increases over time (from $n \approx 2.5$ to $n > 4$), while that of star-forming galaxies remains roughly constant ($n \approx 2.5$). By decomposing galaxy profiles into bulge+disk components, we find that massive galaxies at high redshift have prominent stellar disks, which are also evident from visual inspection of the images. By $z \approx 0.5$, the majority of the disks disappear and massive quiescent galaxies begin to resemble the local elliptical galaxies. Star-forming galaxies have lower bulge-to-total ratios (B/T) than their quiescent counterparts at each redshift bin. The bulges of star-forming and quiescent galaxies follow different evolutionary histories, while their disks evolve similarly. Based on our morphological analysis and previous cosmological simulations, we argue that major mergers, along with minor mergers, have played a crucial role in the significant size increase of high- z galaxies and the destruction of their massive and large-scale disks.

Subject headings: galaxies: spiral and lenticular, cD — galaxies: formation — galaxies: photometry — galaxies: structure — galaxies: surveys

1. INTRODUCTION

Several studies have shown that at $z \approx 2$ a considerable fraction of the massive galaxies (stellar mass $M_\star \approx 10^{11} M_\odot$) are compact compared to their local counterparts (e.g., Daddi et al. 2005; Cimatti et al. 2008; van der Wel et al. 2008; van Dokkum et al. 2008; Damjanov et al. 2009; Hopkins et al. 2009; Cassata et al. 2010, 2011; Mancini et al. 2010; Newman et al. 2012; Szomoru et al. 2012; Williams et al. 2014). The rarity of compact massive galaxies at the present time implies a considerable size increase in the last 10 billion years (van Dokkum et al. 2008; Trujillo et al. 2009; Taylor et al. 2010; van Dokkum et al. 2010; but see Saracco et al. 2010; Valentinuzzi et al. 2010; Ichikawa et al. 2012; Poggianti et al. 2013). Recent comprehensive simulations have found that the commonly used methods for measuring the sizes of these galaxies, such as fitting single-component Sérsic (1968) function, is reliable (e.g., Mosleh et al. 2013; Davari et al. 2014; Davari et al. 2016), despite the fact that, in many instances, their sizes are comparable to the scale of the *Hubble Space Telescope* (*HST*) point-spread function (PSF).

The compactness of high- z massive galaxies strongly suggests that their formation process involved strong

dissipation on rapid timescales (e.g., Naab et al. 2007). This can be accomplished by gas-rich major mergers (e.g., Barnes & Hernquist 1992), cold gas flows (Dekel et al. 2009), or some combination of the two. In support of such a scenario, the central regions of local massive ellipticals, the likely descendants of high- z compact, massive galaxies, are old and have a high α/Fe abundance ratio (Thomas et al. 2005). This indicates an early episode of violent star formation, which would naturally accompany a gas-rich, dissipative formation event. Although major mergers have long been thought to transform disk galaxies to bulge-dominated systems (Toomre 1977; Barnes & Hernquist 1992), more recent simulations show that this may not be always the case. In fact, gas-rich major mergers can leave large-scale disks (Robertson et al. 2006; Hopkins et al. 2009) if the gas retains significant angular momentum during the merger (Springel & Hernquist 2005), especially those that have a high gas fraction (Hopkins et al. 2009).

The study of Toft et al. (2014) lends credence to this picture. These authors show that massive, evolved, compact galaxies at $z \approx 2$ — the so-called red nuggets — are the direct descendants of the submillimeter galaxies (SMGs; Blain et al. 2002) at $z > 3$. SMGs are among the most luminous, rapidly star-forming galaxies known, with luminosities greater than $10^{12} L_\odot$ and star formation rates of $\sim 10^2 - 10^3 M_\odot \text{ yr}^{-1}$ (e.g., Kovács et al. 2006; Magnelli et al. 2010a; Michałowski et al. 2012). Indeed, Toft et al. (2014) show that the mass-size distribution and the mean stellar mass surface density of these two classes of high-redshift galaxies are similar. Both types are best fit by low Sérsic indices (n). Moreover, from a CO study of 30 local merger remnants, Ueda et al.

¹ University of California, Riverside 900 University Avenue, Riverside, CA 92521, USA

² The Observatories of the Carnegie Institution for Science 813 Santa Barbara Street, Pasadena, CA 91101, USA

³ Kavli Institute for Astronomy and Astrophysics, Peking University, Beijing 100871, P. R. China

⁴ Department of Astronomy, School of Physics, Peking University, Beijing 100871, P. R. China

(2014) find that the majority of the sources exhibit kinematic signatures of rotating molecular gas disks. Furthermore, Targett et al. (2013) conclude that more than 95% of SMGs have pure stellar disks or disk-dominated stellar structures; the distribution of axial ratios (their Figure 6) rejects the possibility that the sample is bulge-dominated.

The above arguments strongly suggest that high- z massive galaxies should host large-scale stellar disks. This hypothesis is attested by a number of studies. From the work of van der Wel et al. (2011), 50% of massive galaxies at $z > 2$ are disk-dominated. Similarly, Chang et al. (2013) find that massive galaxies at $z > 1$ have higher axial ratios than their lower redshift counterparts, broadly consistent with the tendency for galaxies to become noticeably rounder between $z \approx 3$ and 0 (Patel et al. 2013).

Now the question remains: how have the red nuggets, which most likely contained a significant disk component at $z \approx 2$ turn, into local giant ellipticals like M87, which demonstrably do *not* have a disk? We aim to trace this morphological transition. We do so by performing detailed two-dimensional modeling of the optical light distribution of massive galaxies within $0.5 < z < 2.5$. Besides fitting a traditional, simple single-component Sérsic function, when possible, we perform a bulge+disk decomposition of these massive systems. Examining separately the bulge and disk structural properties, plus the luminosity bulge-to-total ratio (B/T), provides key indicators that can be missed by studying potentially multiple-component galaxies as a single system. For instance, from the comprehensive morphological analysis by Bruce et al. (2014), massive galaxies appear to transit from disk-dominated to bulge-dominated between $z \approx 3$ and 1, with elliptical-like systems emerge at lower redshifts. The bulge+disk decomposition carried out by Bruce et al. was done by fixing the Sérsic index of the bulge to $n = 4$ and of the disk to $n = 1$. In other words, all bulges were assumed to follow a de Vaucouleurs (1948) light profile. The simulations of Davari et al. (2016) show that this method can lead to biases in measuring the properties of the bulge and disk, depending on the size, S/N , and redshift of the galaxy. For instance, fixing bulge n can overestimate/underestimate the bulge/disk total brightness, and in general, the uncertainties tend to be greater when the bulge n is fixed. Besides, by fixing the bulge Sérsic index, one cannot tell how the bulge density and shape evolve, and important information is lost. Our study relaxes the restriction on the bulge profile shape, which results in more robust and informative bulge+disk decompositions (Davari et al. 2016).

The Cosmic Assembly Near-infrared Deep Extragalactic Legacy Survey (CANDELS; Grogin et al. 2011; Koekemoer et al. 2011)⁵, provides an unprecedented chance to investigate the morphological evolution of galaxies. In fact, one of the original science goals of CANDELS is to trace the bulge and disk growth in rest-frame optical wavelengths at $1 < z < 3$ (Grogin et al. 2011). We take advantage of all wide and deep images taken in five well-known, widely separated fields: GOODS-South and GOODS-North (The Great Observatories Origins Deep Survey; Giavalisco et al. 2004), UDS (UKIDSS

Ultra-Deep Survey; Lawrence et al. 2007), COSMOS (The Cosmic Evolution Survey; Scoville et al. 2007a; Scoville et al. 2007b), and EGS (The Extended Groth Strip; Davis et al. 2007). These collectively yield a statistically uniform and robust sample that mitigates cosmic variance.

The most massive galaxies in the local Universe are almost all quiescent (Baldry et al. 2012), which is not the case at earlier epochs (Whitaker et al. 2011). This means that massive star-forming galaxies have all quenched over time. Quantifying the evolution of both quiescent and star-forming galaxies helps trace back the formation of massive ellipticals and understand the bigger picture.

We address three key questions:

1) How does the size and the shape of the light distribution (Sérsic index) of star-forming and quiescent massive galaxies evolve?

2) Do high-redshift massive galaxies have a prominent stellar disk? If yes, do their relative bulge fraction evolve significantly over the last 10 billion years?

3) What does the observed evolution of bulges and disks teach us about the history of massive galaxies?

Our findings show that the massive galaxies were compact and indeed more disk-dominated at higher redshifts and became more bulge-dominated over time, converging to the population of massive ellipticals by today. Only major mergers can effectively destroy large-scale disks. Thus, while minor mergers were largely responsible for the significant size increase of high- z galaxies, our results underscore that major mergers also played an important role in the morphological transformation of massive galaxies.

This paper is organized as follows. Section 2 provides details of the sample definition, which uses techniques described in Section 3. The morphological analysis is presented in Section 4. Section 5 discusses the implications of our results, and a summary is given in Section 6. Throughout this study we adopt a standard cosmology ($H_0 = 71 \text{ km}^{-1} \text{ s}^{-1} \text{ Mpc}^{-1}$, $\Omega_m = 0.27$, and $\Omega_\Lambda = 0.73$) and AB magnitudes.

2. SAMPLE DEFINITION

We utilize CANDELS images and catalogs. Besides their high-quality near-IR photometry taken with *HST*/WFC3, the observations are complemented with deep *HST*/ACS optical images, mid-IR photometry from *Spitzer*, and near-UV observations from the ground. This provides a reliable dataset for the determination of photometric redshifts and stellar masses.

The photometric redshifts are computed by combining 11 independent measurements (Dahlen et al. 2013), each using different combinations of photometric redshift code, template spectral energy distributions, and priors.

The median fraction difference between the photometric and spectroscopic redshifts is less than 0.01, with an rms scatter of ~ 0.03 (Dahlen et al. 2013). As this study is mostly concerned with broad evolutionary trends between $z \approx 2.5$ to 0.5, precise redshifts for individual objects are not essential to our analysis.

The final quoted stellar mass is the median of estimates from 10 different CANDELS teams, who used the same photometry and redshifts estimates but different fitting codes, assumptions, priors, and parameter grid (Mobasher et al. 2015; Santini et al. 2015). For massive

⁵ <http://candels.ucolick.org/>

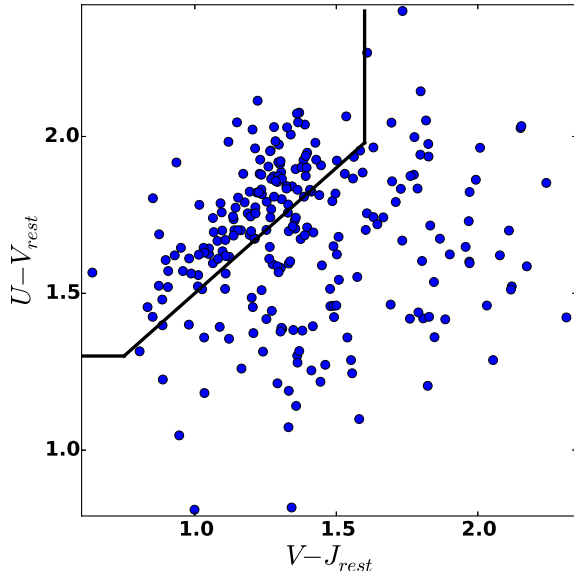


FIG. 1.— UVJ color-color diagram is used for distinguishing quiescent galaxies from star-forming galaxies. The quiescent galaxies populate the top left region of the diagram.

galaxies, there is good agreement between CANDELS and 3D-HST (Skelton et al. 2014; Santini et al. 2015). Mobasher et al. (2015) perform extensive simulations to quantify the different sources of errors and uncertainties, using 10 ten independent methods and mock galaxy catalogs with a range of redshifts, masses, and spectral energy distributions. They concluded that different methods have comparable scatter of 0.136 dex, with no significant bias.

We employ the CANDELS H -band images and the accompanied catalogs to analyze the evolution of the rest-frame optical properties of massive galaxies between $z \approx 2.5$ and 0.5. The observed H magnitudes of our sample range from 24 - 17 mag (measured by Single Sérsic fit), corresponding to the V -band rest-frame of 15.5 - 12 mag. We estimated the rest-frame magnitudes by constructing SEDs of individual galaxies, shifting them to $z=0$, and convolving the resulting rest-frame SEDs with the V -band response function. The high resolution (pixel scale = $0.06''$), bright limiting magnitude ($5\sigma \approx 27$ mag), and wide areal coverage of the CANDELS fields, coupled with the availability of physical parameters (photometric redshift, stellar mass) for individual galaxies, make this dataset unique and ideal for our photometric analysis.

We use the rest-frame UVJ color-color diagram to separate quiescent galaxies from star-forming galaxies (see, e.g., Labbé et al. 2006; Wuyts et al. 2007; Williams et al. 2009; Patel et al. 2013). We use the selection criteria of Patel et al. (2013) to differentiate between these two types of galaxies (Figure 1). Quiescent galaxies populate a region defined by

$$\begin{aligned} U - V &> 1.3 \\ V - J &< 1.6 \\ U - V &> 1.08(V - J) + 0.43, \end{aligned} \quad (1)$$

where U , V , and J are rest-frame magnitudes, calculated using the EAZY photometric redshift code (Brammer et al. 2008) and templates from Muzzin et al. (2013). The fraction of star-forming and quiescent galaxies in our sample at different redshifts is shown in Figure

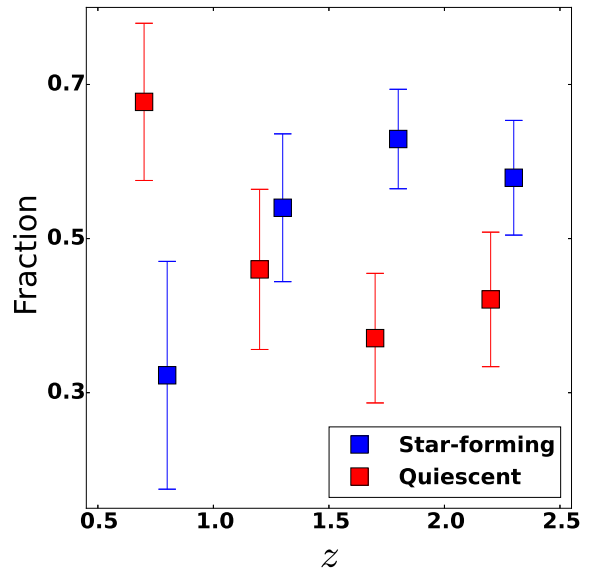


FIG. 2.— Fraction of massive star-forming and quiescent galaxies in redshift range $0.5 < z < 2.5$. Error bars show our sample proportions standard deviation.

TABLE 1
 H -BAND – SELECTED SAMPLE

Redshift Bin (1)	$\log(M_*/M_\odot)$ (2)	N (3)	Quiescent Fraction (4)
$0.5 < z \leq 1.0$	11.02–11.27	31	0.68 ± 0.10
$1.0 < z \leq 1.5$	10.95–11.20	51	0.45 ± 0.10
$1.5 < z \leq 2.0$	10.85–11.10	89	0.37 ± 0.08
$2.0 < z \leq 2.5$	10.74–10.99	77	0.41 ± 0.09

NOTE. — Massive galaxies selected from five different CANDELS fields: COSMOS, UDS, GOODS-South, GOODS-North, & EGS. UVJ diagram is used for distinguishing quiescent from star forming galaxies Col. (2) Redshift bin. Col. (2) Stellar mass range based on constant cumulative number density. Col. (3) Number of galaxies. Col. (4) Fraction of quiescent galaxies.

2 and Table 1. It can be seen that at $z = 2.5$ most massive galaxies were star-forming. By $z \leq 1$, the majority of massive galaxies are quenched, in agreement with the findings of Brammer et al. (2011) and Patel et al. (2013).

We choose massive galaxies based on number density selection rather than a fixed stellar mass limit. For a chosen cumulative number density, we rank galaxies according to their stellar mass and chose galaxies of the same rank at different redshifts. Mundy et al. (2015), using the Millennium Simulation results (Springel et al. 2005; Lemson et al. 2006), show that the former is more reliable for tracing the true evolution of the average stellar mass below $z = 3$. Number density selection, despite its limitations, is more physically motivated (Leja et al. 2013). For instance, red nuggets have doubled their stellar masses in the last 10 billion years (van Dokkum et al. 2010). In other words, local massive galaxies were less massive in the past and could be left out of a fixed stellar mass selection. To trace the evolution of massive galax-

ies, it is more sensible to select galaxies at a constant cumulative number density (van Dokkum et al. 2010; Brammer et al. 2011; Papovich et al. 2011; Patel et al. 2013). We use the criteria of Patel et al. (2013) for selecting galaxies at a fixed cumulative number density, n_c . Their Figure 2 shows that $n_c = 1.4 \times 10^{-4} \text{ Mpc}^{-3}$ corresponds to $M_* = 10^{10.8}$ and $10^{11.1} M_\odot$ at $z = 2.5$ and 0.5 , respectively. Local ($z \approx 0$) galaxies with this corresponding stellar mass ($M_* \approx 10^{11.2} M_\odot$) are predominantly quiescent (van der Wel et al. 2009; Baldry et al. 2012) and have large axial ratios (van der Wel et al. 2009), and therefore massive ellipticals.

Our sample consists of ~ 250 massive galaxies, whose properties are summarized in Table 1. The mass range for each redshift bin takes into account systematic uncertainties in the stellar mass estimate.

3. GALFIT MODELING

We use **GALFIT** 3.0 (Peng et al. 2010) as the main modeling tool. **GALFIT** is a powerful, simple-to-use image analysis code to fit the light distribution of galaxies and other objects. Of the several available options, we mainly use the Sérsic (1968) function to fit the surface brightness distribution:

$$\Sigma(R) = \Sigma_e \exp \left\{ -\kappa \left[\left(\frac{R}{R_e} \right)^{1/n} - 1 \right] \right\}, \quad (2)$$

where Σ_e stands for the surface brightness, R_e is the half-light (effective) radius, n is the Sérsic index that governs the shape of the profile, and κ is a variable that depends on n (Ciotti 1991). The Sérsic function is a generalization of the special cases of an exponential profile ($n = 1$) used to model disks (Freeman 1970) and the $R^{1/4}$ law ($n = 4$) traditionally used to model elliptical galaxies and bulges (de Vaucouleurs 1948). Modern studies recognize that ellipticals and bulges have a more varied range of n (e.g., Caon et al. 1993; Andredakis & Sanders 1994; Blanton et al. 2003; Fisher & Drory 2008).

Several inputs are needed to perform fit: a PSF model, a “sigma” image, and (sometimes) a bad pixel mask. For each galaxy, we use the *H*-band CANDELS hybrid PSF corresponding to its field (e.g., UDS, COSMOS, etc.; van der Wel et al. 2012). Hybrid PSFs are built by combining a stacked empirical stellar PSF and a synthetic **TinyTim** (Krist et al. 2011) PSF. CANDELS weight maps are used as the input sigma images. As the field around each galaxy is chosen to be more than 10–15 times larger than the size of the galaxy, there are usually several other objects in the field that need to be masked. As in Davari et al. (2014), we use **SExtractor**⁶ (Bertin & Arnouts 1996) to identify bright field objects and create a bad pixel mask that covers twice the area detected by **SExtractor**.

For any given galaxy in the sample, our primary goal is to ascertain whether its light distribution, apart from a central bulge, shows evidence for an additional disk component, and if so, to determine its relative light fraction. We model each galaxy twice, first with a single-component Sérsic fit, and then with a two-component fit consisting of a bulge and a disk. The bulge is assigned

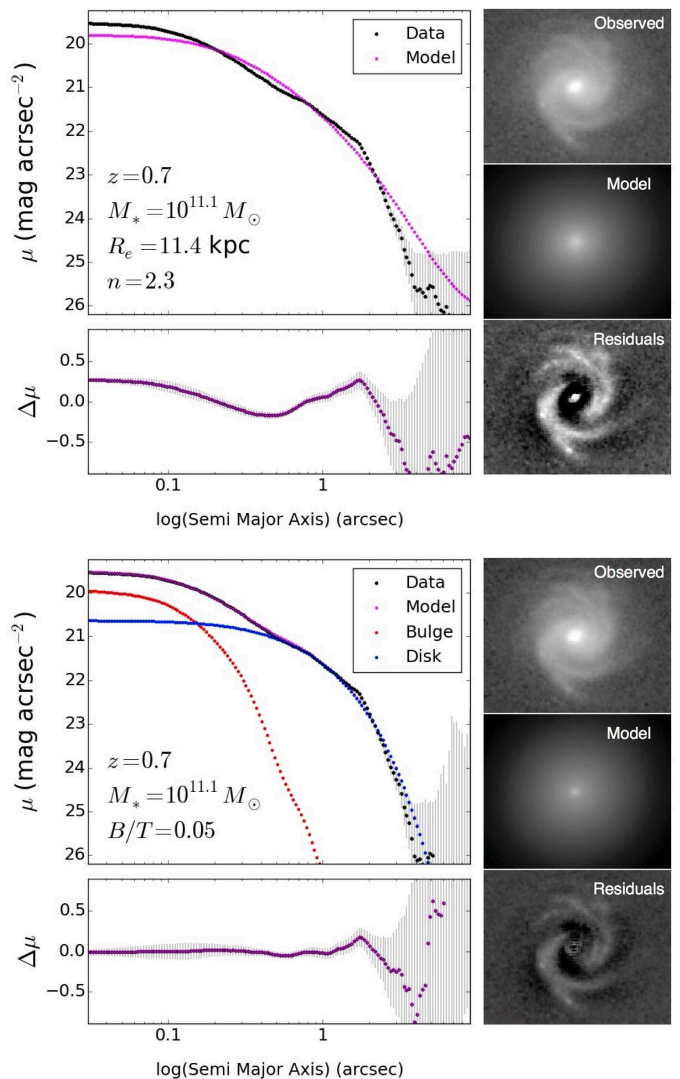


FIG. 3.— Diagnostic plots used to examine the goodness of a fit. Top left panels show the mean surface brightness (μ) profile of the galaxy, the **GALFIT** fit model, and the bulge and disk components (in cases of bulge+disk decomposition). Bottom left panels show the residuals between the model and the observed mean surface brightness. The error bars are calculated using the RMS of the image background and the surface brightness measurement error calculated by **ellipse** in **IRAF**. The right panels, from top to bottom, show the observed galaxy, the **GALFIT** model, and the residuals, respectively. The top panel makes it clear that the fitted galaxy has a bulge-line central concentration and spiral arms, and hence a disk; the model is trying to accommodate both components. The bottom light profile plots show that the bulge+disk decomposition reproduces the light profile of the galaxy well.

a Sérsic function with n allowed to vary, and the disk fixed to an exponential. We then carefully examine the residuals to determine the merits of the two models.

Depending on the complexity of the **GALFIT** model, the initial parameters (guesses) can have a large effect on the fit. For single-component fits, unless the initial guesses are very far off the actual values, the initial parameters do not have a major effect. Regardless, we use one-dimensional light profiles obtained by **IRAF/ellipse** (Jedrzejewski 1987) to obtain reliable initial guesses. We construct a curve-of-growth of the light distribution to estimate the effective radius, total luminosity, axial ratio, and position angle (for more details, see Davari et al.

⁶ <http://www.astromatic.net/software/sextractor>

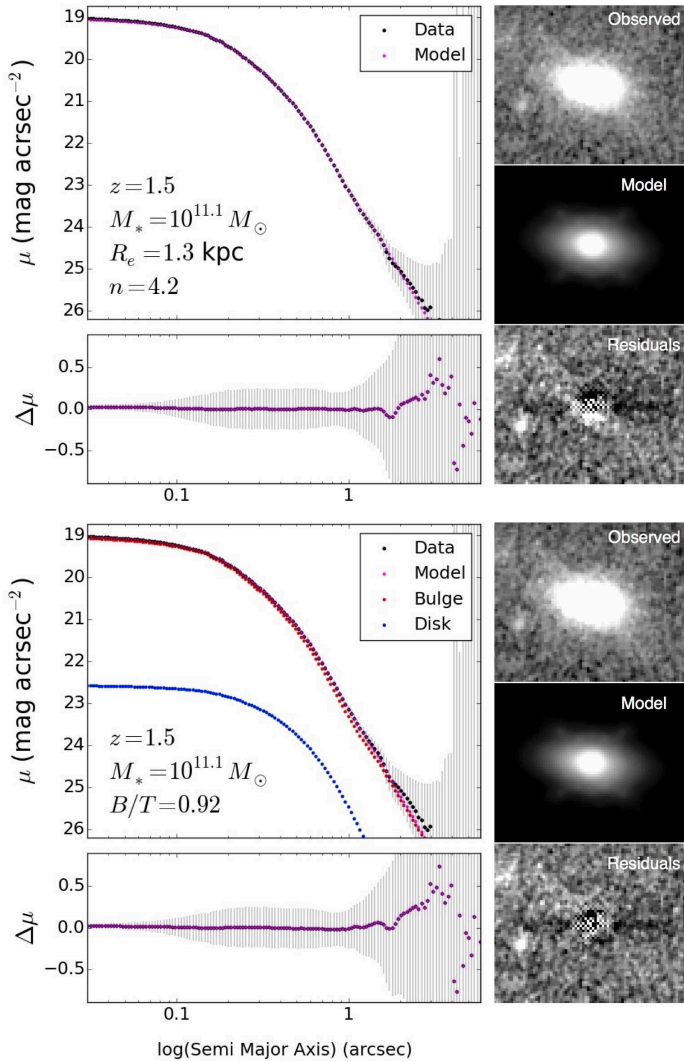


FIG. 4.— Similar to Figure 3. This galaxy is basically a single spheroidal, and adding a second component does not improve the model fit significantly.

2014). Appropriate initial guesses become much more important for the bulge+disk decompositions. For this type of modeling, we again use the one-dimensional light profile to obtain initial inputs. Assuming that the disk component follows an approximately exponential profile, we look for the part of the profile that traces a straight line in logarithmic space. Depending on the B/T , this region is located between 2 and 5 R_e , where the effect of the bulge is minimal. A straight line fitted to that section of the light distribution (in logarithmic space) provides an estimate for the disk scale length and central surface brightness. The total brightness obtained from a single Sérsic fit is used to find the total luminosity of the bulge component, and therefore B/T . Each galaxy is fit numerous times with different initial guesses for bulge R_e and n , in addition to all the estimated parameters. While fitting a single Sérsic function might require only a few iterations, bulge+disk decompositions can require several fits with different initial guesses. The diagnostic plots (explained below) are imperative for evaluating the goodness of a fit. Lastly, the fitted sky component is left as a free parameter, and its initial values are set to

zero. The simulations performed by Davari et al. (2014) and Davari et al. (2016) show that once the field size of the image is more than 10 times larger than the galaxy, GALFIT can measure the sky reliably.

Figures 3 and 4 give examples of the diagnostic plots used to examine the goodness of a fit and whether or not a second component is needed. The top left panels show the mean one-dimensional surface brightness (μ) profile of the galaxy, the final GALFIT model, and the bulge and, if necessary, the disk components. The bottom left panels show the residuals (model – galaxy). The error bars are calculated using the rms of the image background and the galaxy flux measurement error (output from *ellipse*). The right panels, from top to bottom, illustrate the two-dimensional image of the galaxy, model, and residuals.

The top right panel of Figure 3 clearly reveals that the galaxy, in addition to a bright central concentration, has a disk and spiral arms. The one-dimensional profile in the left panel confirms that the galaxy contains complex structure. The single-component model is trying to capture the most of the combination of two components, but the fit is clearly inadequate. The bulge+disk decomposition, by contrast, reproduces well the μ profile on the bottom left panel. And not surprisingly, this galaxy is extremely disk-dominated: the best fit yields $B/T = 0.05$. At the other extreme, Figure 4 showcases a galaxy that is basically a just single big bulge; adding a second component does not improve the fit significantly. The high B/T of this galaxy (0.92) validates this hypothesis.

Davari et al. (2014, 2016) demonstrate that large Sérsic indices ($n > 6$) derived from single-component fits can lead to significant biases, which can be remedied by fixing n to 6, after testing the fit for different initial guesses. This study follows the same general rule, except that the diagnostic plots are given more weight. For example, if fixing n to 4 or 8 gives a better fit and cleaner residuals than fixing n to 6, then those values are used. Another common symptom of unreliable fits is when the effective radius of the bulge drops below 0.5 pixel. For many of these cases, changing the initial guesses of R_e and n leads to more realistic solutions. But if the problem persists, we resort to fixing the bulge R_e (or sometimes n or both) to different initial values, and we rely on visual inspection of the residuals to judge the merit of each model. For about 25% of the galaxies at $z > 1.5$, the bulge R_e (mainly to $R_e=1$) and/or bulge Sérsic index (mainly to $n=1$) are fixed.

In short, the goodness of single and two component fits are mainly determined by visual inspection of the residual images (galaxy - model), along with the derived Sérsic profile parameters. The derived Sérsic parameters of each component have to be reasonable for a fit (e.g., $R_{e\text{bulge}}/R_{e\text{disk}} < 1$, ellipticities < 0.8 , sizes > 0.5 pixel, and etc.) to be considered reliable. The objective of this study is not fitting two components only when there is an improvement over the single Sérsic fit residual. For example, Figure 4 shows an example of a bulge-dominated galaxy, where adding a second component does not improve the residual significantly. However, the derived two component fit parameters not only confirm that this galaxy is bulge dominated (high B/T), but also provides additional information (e.g., $R_{e\text{bulge}}$, n_{bulge} , h , and etc.) Out of 248, only 1 and 7 galaxies could not be fit reliably

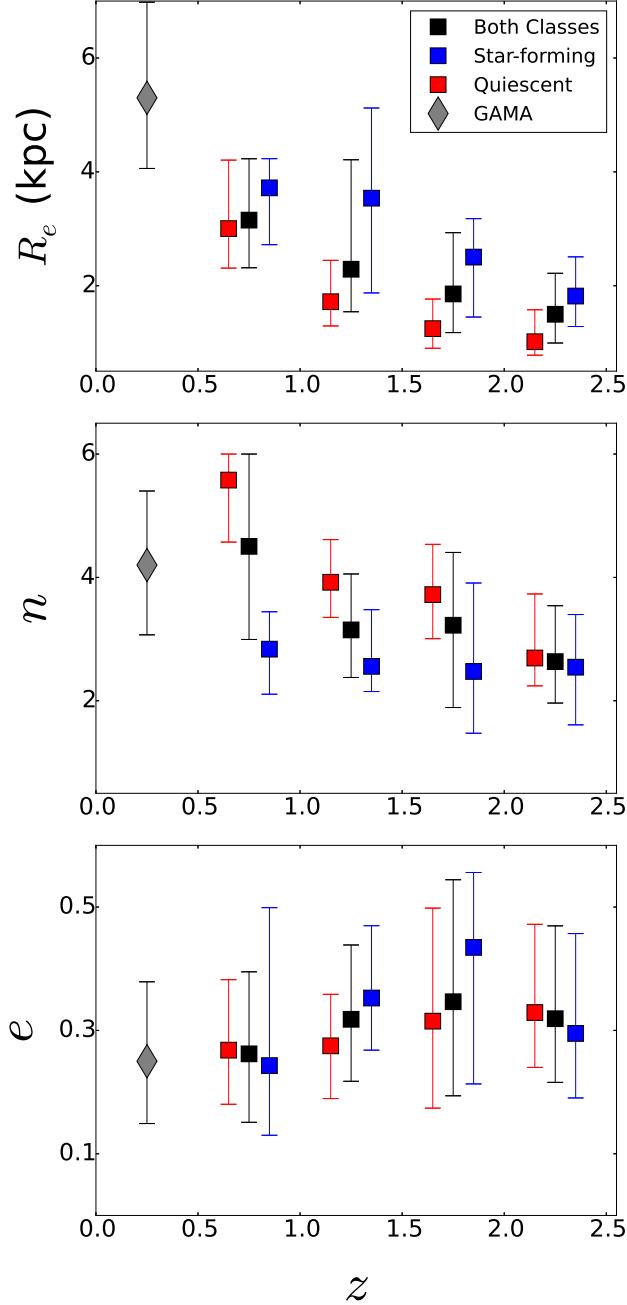


FIG. 5.— Results of single Sérsic fits. Top, middle, and bottom panels show the redshift evolution of effective radius (R_e), Sérsic index (n), and ellipticity (e). Red, blue, and black filled boxes show the median in each redshift bin for quiescent galaxies, star-forming galaxies, and both types combined. The gray filled diamond shows the median value for a sample from the second data release of GAMA (Driver et al. 2009; Liske et al. 2015) with mass range corresponding to our number density selection criteria. Their morphological parameters are derived from single Sérsic fits, consistent with our method. The error bars correspond to the interquartile range of different measurements.

with a single Sérsic and two components, respectively, and are omitted from the following analysis. In most of these cases, the image contains multiple regions with nonuniform and anomalous background values.

TABLE 2
STATISTICAL TESTS OF SINGLE SÉRSIC FITS

Variable	ANOVA		KS	
	F -value	p -value	D -value	p -value
(1)	(2)	(3)	(4)	(5)
R_e	20.39	$<10^{-11}$	0.28	$<10^{-4}$
n	9.98	$<10^{-5}$	0.35	$<10^{-6}$
e	1.66	0.18	0.15	0.14

NOTE. — Col. (1) Parameters measured using Single Sérsic fitting. Col. (2) (variance of sample means at different redshift bins) / (variance of the whole sample) Col. (3) The ANOVA test p -values. Small p -values (< 0.05) reject the null-hypothesis that the means values are not statistically different at different redshift bins. Col. (4) The maximum difference between the empirical cumulative distribution functions of the two samples. Col. (5) The KS test p -values. Small p -values (< 0.05) reject the null-hypothesis that the two samples are drawn from the same distribution.

TABLE 3
QUANTIFYING SIZE EVOLUTION

Variable	Quiescent	Star-forming	Both
R_e	-1.75 ± 0.16	-1.17 ± 0.31	-1.19 ± 0.03
$R_{e,\text{bulge}}$	-2.55 ± 0.43	-1.61 ± 0.17	-2.38 ± 0.43
h	-1.60 ± 0.07	-1.14 ± 0.15	-1.27 ± 0.06

NOTE. — Evolution of the global effective radius (R_e), bulge effective radius ($R_{e,\text{bulge}}$), and disk scale length (h), parameterized as a function of $(1+z)^\alpha$. The values of α for the star-forming, quiescent, and both classes are listed. The R_e , $R_{e,\text{bulge}}$, and h are derived from the fitted Sérsic profiles (Equation 2) and in turn, are converted to physical sizes (kpc) before quantifying the size evolution.

4. RESULTS

4.1. Fitting Galaxies with Single Sérsic Component

Single Sérsic fitting is probably the most widely adopted method in the literature for morphological studies. This method provides a rather straightforward way for evaluating some key morphological properties of galaxies, namely size (usually parameterized as the effective radius; R_e), Sérsic index (n), and ellipticity (e). For instance, if a randomly distributed galaxy population has a significant disk component, we expect a wide distribution of n and e . The simulations of Davari et al. (2014, 2015) show that single-component fits of massive galaxies at the redshift range of current interest ($0.5 < z < 2.5$)

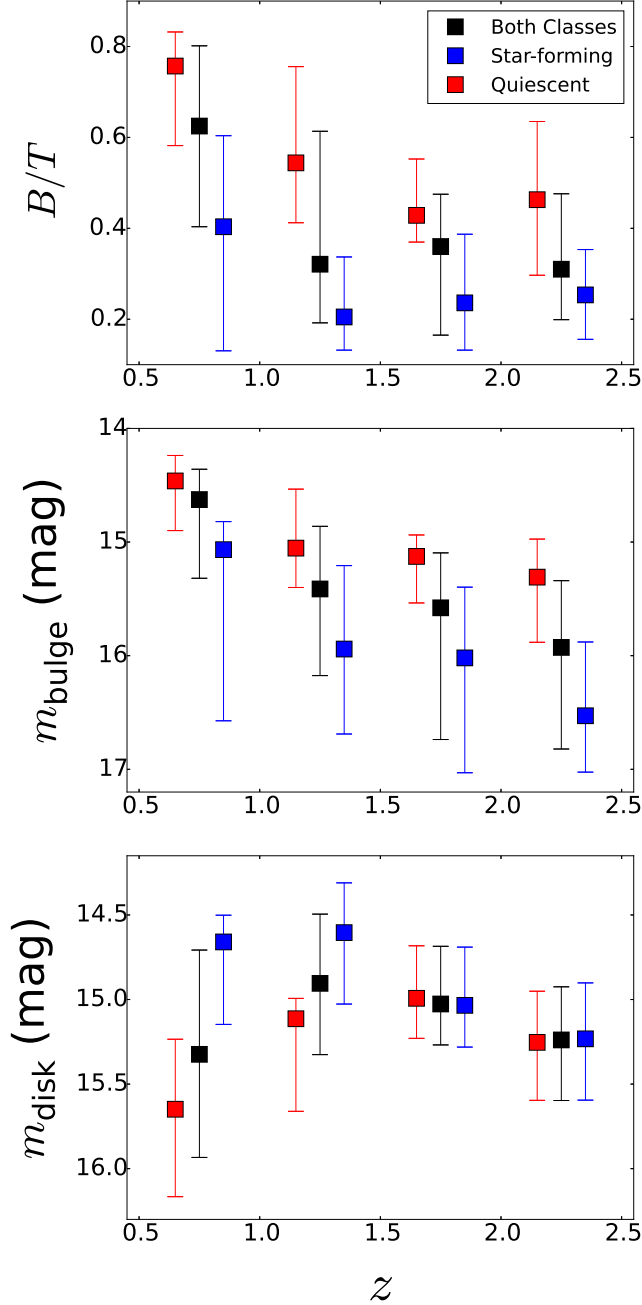


FIG. 6.— Results of bulge+disk decomposition. Top, middle, and bottom panels show the redshift evolution of flux bulge-to-total ratio (B/T), bulge magnitude (m_{bulge}), and disk magnitude (m_{disk}). The reported magnitudes are rest-frame magnitude in V-band. Red, blue, and black filled boxes show the median in each redshift bin for quiescent galaxies, star-forming galaxies, and both types combined. The error bars correspond to the interquartile range of different measurements.

can be measured with little to no systematic uncertainty.

Figure 5 summarizes the results of single-component fits of our sample, highlighting the redshift evolution of R_e , n , and e , separately for quiescent and star-forming galaxies. For reference, we overplot the median value for a sample drawn from the second data release of GAMA (Driver et al. 2009; Liske et al. 2015); the sample mass

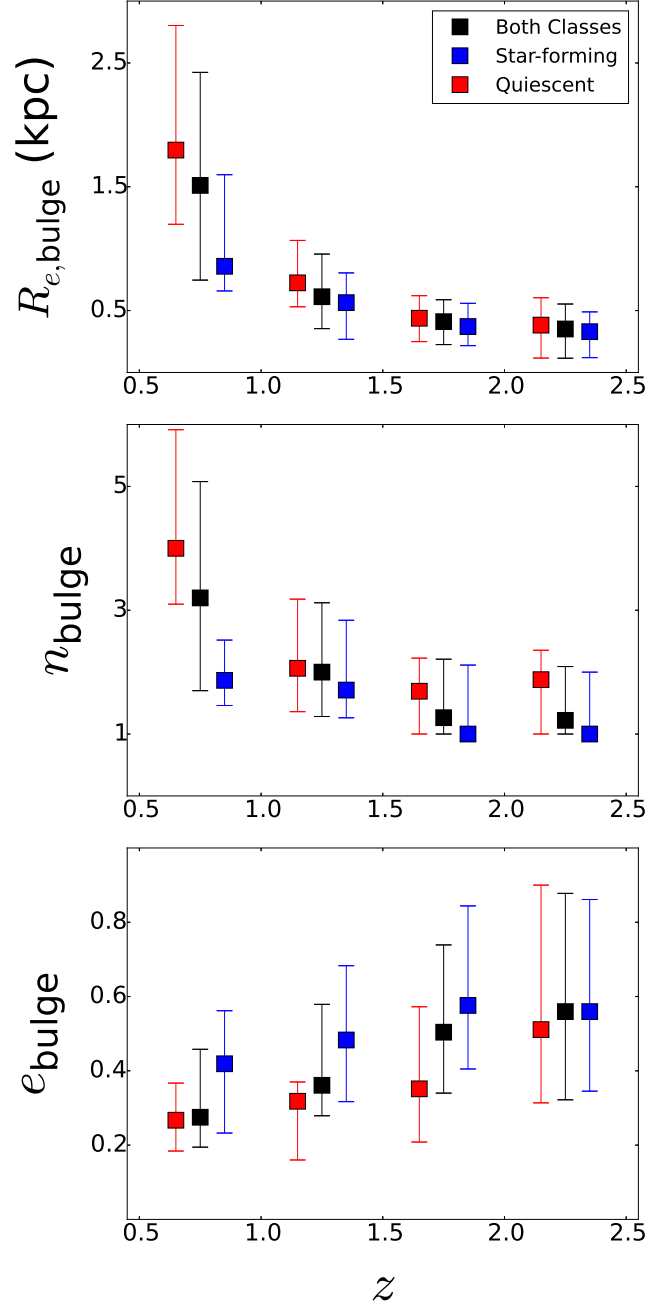


FIG. 7.— Results of bulge+disk decomposition. Top, middle, and bottom panels show the redshift evolution of bulge effective radius ($R_{e,\text{bulge}}$), bulge Sérsic index (n_{bulge}), and bulge ellipticity (e_{bulge}). Red, blue, and black filled boxes show the median in each redshift bin for quiescent galaxies, star-forming galaxies, and both types combined. The error bars correspond to the interquartile range of different measurements.

range corresponds to our number density selection (i.e. $M_{\star} = 10^{11.1} - 10^{11.3} M_{\odot}$) at $0 < z < 0.5$. The morphological parameters of the GAMA survey are derived by single Sérsic fitting, consistent with our method. The error bars correspond to the interquartile range of different measurements.

We perform two statistical tests to quantify the significance of the observed evolution of different properties:

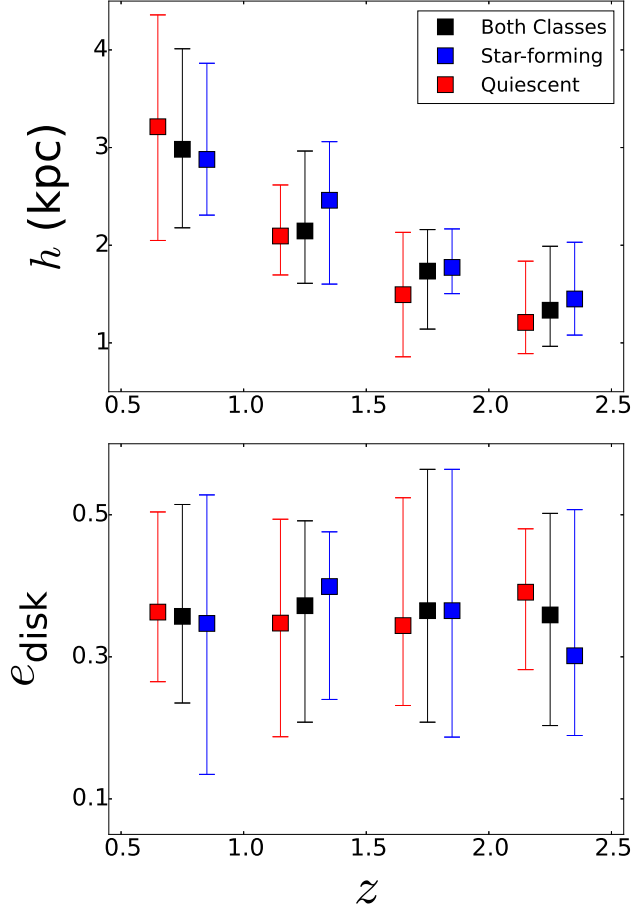


FIG. 8.— Results of bulge+disk decomposition. Top and bottom panels show the redshift evolution of disk scale length (h) and disk ellipticity (e_{disk}). Red, blue, and black filled boxes show the median in each redshift bin for quiescent galaxies, star-forming galaxies, and both types combined. The error bars correspond to the interquartile range of different measurements.

two-sample Kolmogorov-Smirnov (KS) test and one-way analysis of variance (ANOVA). The KS test is used to determine whether the star-forming and quiescent samples are drawn from the same parent population. As a non-parametric test, it has the advantage of making no assumption about the distribution of data. The results of KS test are summarized by the D -value and the p -value. The D -value shows the maximum difference between the empirical cumulative distribution functions of the two samples, while the p -value indicates the significance of the difference between two samples. Small p -values (< 0.05) reject the null hypothesis that the two samples are drawn from the same distribution. ANOVA tests whether there are any statistically significant differences between the means of sample quantities in our redshift bins. The F -value (i.e. F statistics) quantifies the variance between groups compared to the variance within groups: (variance of sample means at different redshift bins)/(variance of the whole sample). High F -values (i.e., small p -values) reject the null-hypothesis that the mean values are not statistically different at different redshift bins. In this study, high F -values indicate there is evolution over the observed redshift range.

TABLE 4
BULGE+DISK DECOMPOSITION STATISTICAL TESTS RESULTS

Variable (1)	ANOVA		KS	
	F -value (2)	p -value (3)	D -value (4)	p -value (5)
B/T	13.36	$<10^{-7}$	0.49	$<10^{-12}$
m_{bulge}	12.93	$<10^{-7}$	0.49	$<10^{-12}$
m_{disk}	6.93	$<10^{-3}$	0.22	$<10^{-2}$
$R_{e,\text{bulge}}$	30.77	$<10^{-16}$	0.21	$<10^{-2}$
n_{bulge}	17.92	$<10^{-9}$	0.24	$<10^{-3}$
e_{bulge}	9.10	$<10^{-9}$	0.34	$<10^{-5}$
h	32.38	$<10^{-16}$	0.11	0.40
e_{disk}	0.09	0.97	0.10	0.51

NOTE. — Col. (1) Parameters measured using the bulge+disk decomposition. Col. (2) (variance of sample means at different redshift bins) / (variance of the whole sample) Col. (3) The ANOVA test p -values. Small p -values (< 0.05) reject the null-hypothesis that the means values are not statistically different at different redshift bins. Col. (4) The maximum difference between the empirical cumulative distribution functions of the two samples. Col. (5) The KS test p -values. Small p -values (< 0.05) reject the null-hypothesis that the two samples are drawn from the same distribution.

The results of the KS and ANOVA test for the single-component fits are listed in Table 2.

Massive galaxies have experienced significant size evolution (top panel of Figure 5; Table 2), with the size increase being more prominent for quiescent galaxies (Table 3). Quiescent galaxies have increased their sizes by a factor of 3 down to $z = 0.5$, and more than a factor of 5 by $z \approx 0$. By contrast, star-forming galaxies have undergone more modest size growth, by a factor of ~ 3 down to $z = 0.5$. However, the absolute amount of size increase between $z = 2.5$ and $z = 0.5$ for both star-forming and quiescent galaxies is comparable, about 2 kpc. The slope of the size-mass relation is consistent with the value found in van Dokkum et al. (2010) and Patel et al. (2013). On average, the size interquartile ranges are smaller for quiescent galaxies, which indicates a greater size diversity among star-forming galaxies. In other words, the sizes of quiescent galaxies are more homogeneous. Furthermore, the star-forming galaxies at each redshift are larger than their quiescent counterparts, in agreement with previous similar studies (e.g., Zirm et al. 2007; Szomoru et al. 2011; Whitaker et al. 2011; Patel et al. 2013; Williams et al. 2014). Star-forming and quiescent galaxies have statistically different size distributions (Table 2).

The global Sérsic indices of both star-forming and quiescent galaxies in our highest redshift bin cluster around $n \approx 2.5$ (middle panel of Figure 5), an intermediate

TABLE 5
ESTIMATED FRACTION OF MASSIVE GALAXIES WITH A PROMINENT STELLAR DISK
USING DIFFERENT DIAGNOSTICS

redshift bin	$B/T \leq 0.5$ (1)			Spiral Structures (2)			Edge-on Disks (3)		
	Quiescent	Star-forming	Both	Quiescent	Star-forming	Both	Quiescent	Star-forming	Both
$0.5 < z \leq 1.0$	0.17 ± 0.07	0.67 ± 0.11	0.36 ± 0.07	0.05 ± 0.04	0.30 ± 0.14	0.13 ± 0.06	0	0.40 ± 0.15	0.13 ± 0.06
$1.0 < z \leq 1.5$	0.50 ± 0.12	0.86 ± 0.06	0.72 ± 0.06	0	0.67 ± 0.09	0.37 ± 0.07	0.35 ± 0.10	0.74 ± 0.08	0.56 ± 0.07
$1.5 < z \leq 2.0$	0.64 ± 0.09	0.90 ± 0.04	0.81 ± 0.05	0	0.18 ± 0.05	0.11 ± 0.03	0.48 ± 0.09	0.50 ± 0.07	0.49 ± 0.05
$2.0 < z \leq 2.5$	0.53 ± 0.09	0.93 ± 0.04	0.77 ± 0.05	0	0.05 ± 0.03	0.03 ± 0.02	0.50 ± 0.09	0.36 ± 0.07	0.42 ± 0.06

NOTE. — Col. (1) Massive galaxies with bulge-to-total ratios less than 0.5. Col. (2) Massive galaxies with visually detectable spiral structures. Col. (3) Edge-one massive galaxies with $e > 0.6$.

value consistent with a composite bulge+disk system. But over time, the two galaxy types diverge (Table 2). While star-forming galaxies maintain an almost constant n , the Sérsic indices of quiescent galaxies increases significantly and systematically toward lower redshifts, eventually converging to resemble those of local elliptical galaxies ($n > 4$) at the lowest redshift bin. These trends are broadly consistent with the results of Morishita et al. (2014), Patel et al. (2013), and Szomoru et al. (2011).

The trends with regards to ellipticity are less definitive. If massive galaxies initially host a sizable disk, we expect the eventual disappearance of that component to produce a notable reduction in the typical ellipticity of the population. In practice, however, the presence of a sizable bulge concentration severely dilutes the expected ellipticity signature of any disk component. Indeed, neither the ANOVA nor the KS test indicates any statistically significant redshift evolution of e . (Table 2). However, considering only the quiescent galaxies at $z > 1.5$ and $z < 1.5$, there are two suggestive indicators of ellipticity evolutions. First, F-test of equality of variances gives a p-value of 0.08 which is a bordering signature of greater range (variance) of ellipticities at $z > 1.5$. Second, comparing ellipticities of the quiescent galaxies at $z > 1.5$ and $z < 1.5$ shows a tentative drop in the overall ellipticity: the two sample one-sided t-test gives a p-value of 0.05. These signatures are suggestive and not conclusive. The following section presents a more detailed analysis which provides an independent gauge for the presence of a disk among massive quiescent galaxies at higher redshifts.

To summarize the results and implications of the single-component fits: the global light distribution of the massive galaxy population evolves significantly from $z = 2.5$ to $z = 0.5$. Apart from the well-known increase in size, the population as a whole, and in particular the quiescent systems, exhibits systematical evolution toward larger Sérsic indices and lower ellipticities at lower redshifts, converging to typical values of local ellipticals. These trends support the thesis that the progenitors of present-day ellipticals were born with a sizable large-scale disk, which over time has been transformed.

4.2. Fitting Galaxies with Two Components

While single Sérsic fitting provides a reliable first-order estimate of morphological properties, decompos-

ing a galaxy into its bulge and disk components can reveal a new set of valuable galaxy evolution indicators. The simulations of Davari et al. (2016) show that gross photometric properties, in particular B/T , of bulge+disk systems usually can be measured accurately, up to $z \approx 2 - 2.5$, without imposing any constraints on the profile shape of the bulge. However, due to the inherent limitations of resolution, even with *HST*, detailed properties of the bulges (e.g., R_e or n) can be measured reliable only for galaxies with $B/T \geq 0.2$. The disk component, by contrast, can be measured with little difficulty.

Figure 6 depicts the overall variation of B/T with redshift for our sample. At higher redshifts, quiescent galaxies have intermediate values of B/T (~ 0.4), but over time they become more and more bulge-dominated. At the lowest redshift bin, $B/T \approx 0.8$, very close to the median value of local massive elliptical galaxies. Although star-forming galaxies, too, become more bulge-dominated with time, their B/T at all redshift bins are lower than that of their quiescent counterparts; the two classes have statistically different distributions in B/T (Table 4). Bruce et al. (2012) report that massive galaxies at $z > 2$ are mostly disk-dominated and by $1 < z < 2$ have increased their B/T to intermediate values, with very few elliptical-like galaxies down to $z = 1$. They show that disk-dominated galaxies have higher star formation rates, which translates into star-forming galaxies having a lower B/T . Similarly, Lang et al. (2014) also find that massive galaxies increase in B/T between $1.5 < z < 2.5$ and $0.5 < z < 1.5$.

Although *H*-band images of galaxies at different redshifts capture the flux in different rest-frame bands (i.e., approximately *V* to *I* band), multi-wavelength studies of nearby galaxies find that B/T does not strongly depend on observed rest-frame wavelength, at least within the standard optical bands (e.g., Schulz et al. 2003; Graham & Worley 2008). The observed variation of B/T between different bands is less than ~ 0.1 . The shallow color gradients of quiescent galaxies (e.g., Wirth 1981) further minimizes the impact of rest-frame wavelength on B/T .

While the bulges of both types of galaxies become more luminous over time, the disks component behaves markedly differently: it becomes sub-dominant

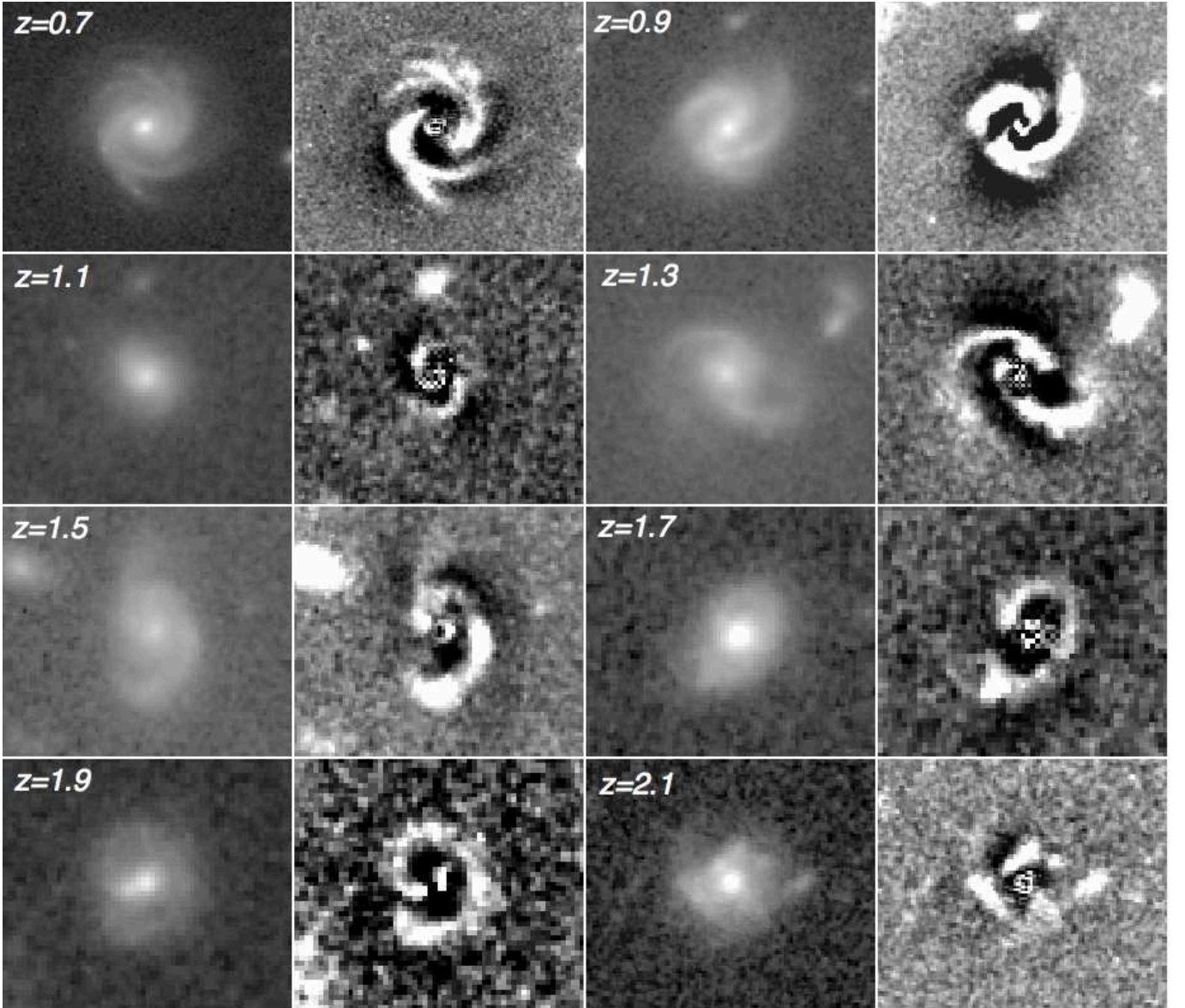


FIG. 9.— Examples of galaxies with apparent spiral structures at different redshifts. The residual images, after removal of the bulge+disk model from the original galaxy image, allows for more effective detection of fine substructure.

in quiescent galaxies but brightens for the star-forming group (middle and bottom panels of Figure 6; Table 4). Meanwhile, the star-forming galaxies disks are becoming brighter at lower redshift bins. The bulges of quiescent galaxies attain higher luminosities than in star-forming galaxies at all redshifts, and in the lowest redshift bin the luminosities of quiescent galaxies have significantly smaller scatter than in star-forming galaxies.

Our bulge+disk decomposition (Figure 7 and Table 3) reinforces the size evolution observed in the single-component fits (Figure 5). The effective radii of the bulges of both classes have grown, and, once more, the evolution is steeper for quiescent galaxies. The disk scale lengths of both star-forming and quiescent galaxies have increased (Figure 8) as well, but their distributions are not distinguishable (Table 4). Table 3 indicates that the disk size increase is less significant compared to the bulge component.

As shown in Figure 7, the Sérsic indices of quies-

cent galaxy bulges have increased considerably but have stayed almost the same for the star-forming population. This is similar to the results of single-component analysis (Figure 5). By redshift 0.5, bulges of quiescent galaxies have Sérsic indices similar to that of typical local ellipticals and classical bulges (Fisher & Drory 2008).

The disk ellipticities of both classes have similar distribution and have not changed between $z = 2.5$ and 0.5 . On the other hand, the bulges of massive galaxies have become rounder over this period. Quiescent galaxies have lower bulge ellipticities, and by $z = 0.5$, their distribution is similar to that of local massive ellipticals and classical bulges (Fathi & Peletier 2003).

In related studies, Bruce et al. (2014a, 2014b) analyze the rest-frame optical morphologies of a mass-selected sample of massive ($M_* > 10^{10.5} M_\odot$) galaxies at $1 < z < 3$ in the CANDELS UDS and COSMOS fields. Similar to our work, they decomposed H_{160} -band images of massive galaxies into their bulge and disk components.

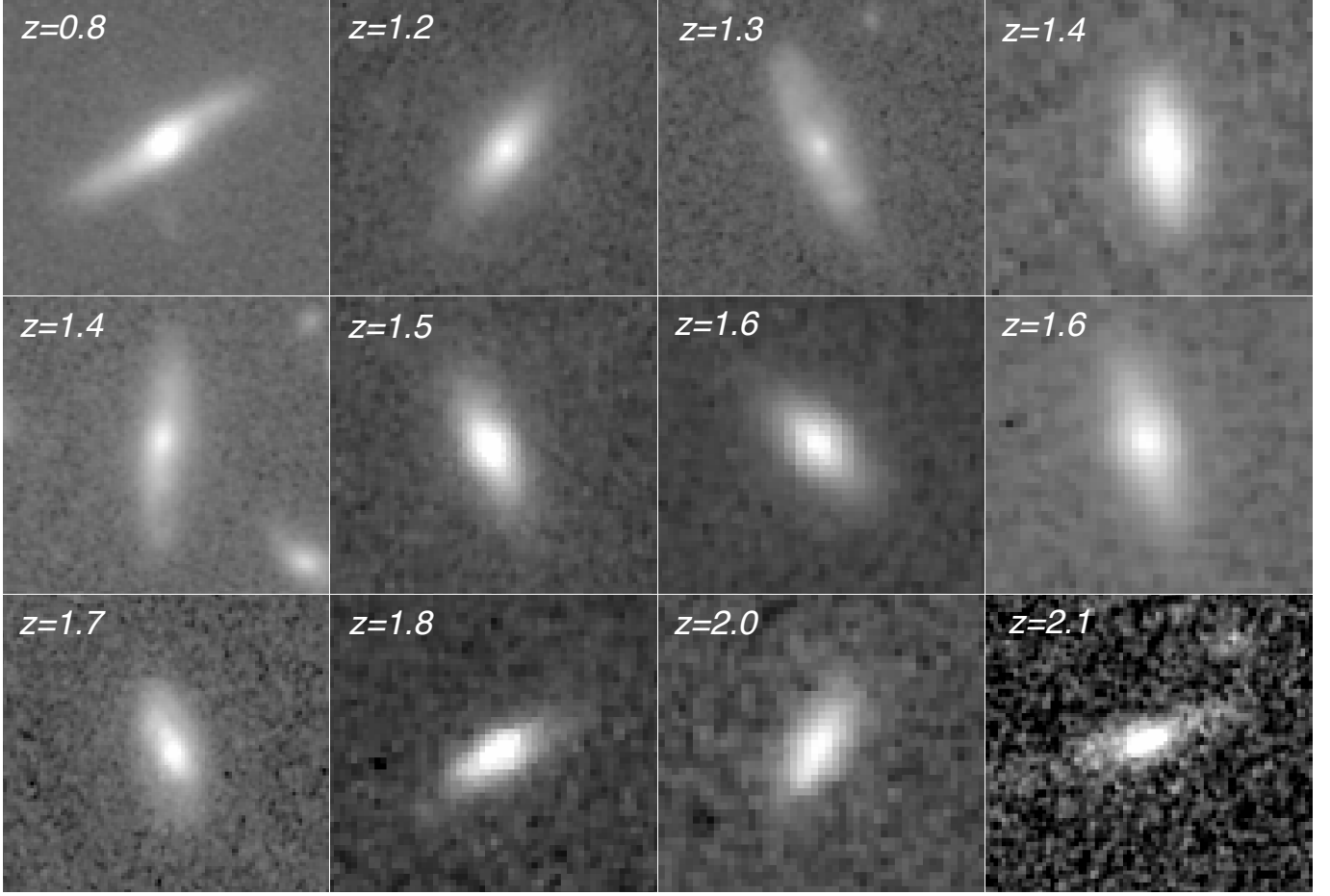


FIG. 10.— Examples of massive galaxies with an edge-on disk at different redshifts.

In general, our results are in agreement with those of these authors. Bruce et al. (2014a) find that from $z = 3$ to $z = 1$ the galaxies transition from disk-dominated to more bulge-dominated (their Figure 6), in accordance with our findings (our Figure 6). The results of Bruce et al. (2014b) show that bulges exhibit a stronger size evolution than disks (their Table 3), with star-forming galaxies having relatively larger disk sizes compared to passive systems (their Figure 8), in qualitative agreement with our results (compare with our Table 3 and Figure 8). However, with regards to the bulge components, they show that star-forming galaxies have larger bulges than quiescent galaxies, contrary to the results from our study. This may be due to the fact that the bulge-disk decomposition of Bruce et al. (2014a, 2014b) was done by fixing the Sérsic index of the bulge and disk components to 4 and 1, respectively. As demonstrated in Davari et al. (2016), fixing the Sérsic indices can lead to biases and larger uncertainties in measuring bulge and disk properties, depending on their size, redshift, and S/N . Furthermore, assuming a fixed profile for disks and bulges at all redshifts precludes any investigation of the evolution of these parameters with look-back time.

4.3. Further Evidence of Prominent Stellar Disks: Detection of Spiral Structures and Edge-on Disks

Despite the prevalence of spiral structures and bars in the local Universe (e.g., Lintott et al. 2011; Willett et al.

2013), these features are not believed to be common among star-forming galaxies at higher redshifts ($z > 1.5$) (e.g., Conselice et al. 2005; Bournaud & Elmegreen 2009; Conselice et al. 2011), where the disks may be too dynamically hot (Genzel et al. 2006; Law et al. 2007; Law et al. 2009).

Our model-subtracted residual images yield an unexpected surprise: a sizable fraction of the sources exhibit spiral structure (Figure 9)⁷. All the cases are star-forming galaxies; there are no quiescent galaxies with securely detectable spiral structure (Table 5). The case with the highest redshift is at $z = 2.4$. The fraction of star-forming galaxies with spiral structure is $\sim 20\%$ at $1.5 < z < 2.0$, and by $1.0 < z < 1.5$, the spiral fraction reaches nearly 70%. The fraction of star-forming galaxies with spiral structures drops (to 30%) at the lowest redshift bin. This decline may not be reliable for two reasons. First, the star-forming sample size at $0.5 < z < 1.0$ is very small (only 10 objects), and therefore the sample proportions are not statistically significant. Second, the H -band images for the low- z objects are missing the bluer parts of the galaxy flux (see also Elmegreen & Elmegreen 2014).

The conditions necessary for the formation of spiral arms are complex (see Dobbs & Baba 2014 for a review), but one requirement is clear—the existence of a disk.

⁷ Some examples can also be seen in Figures C1 and C3 of Bruce et al. (2012).

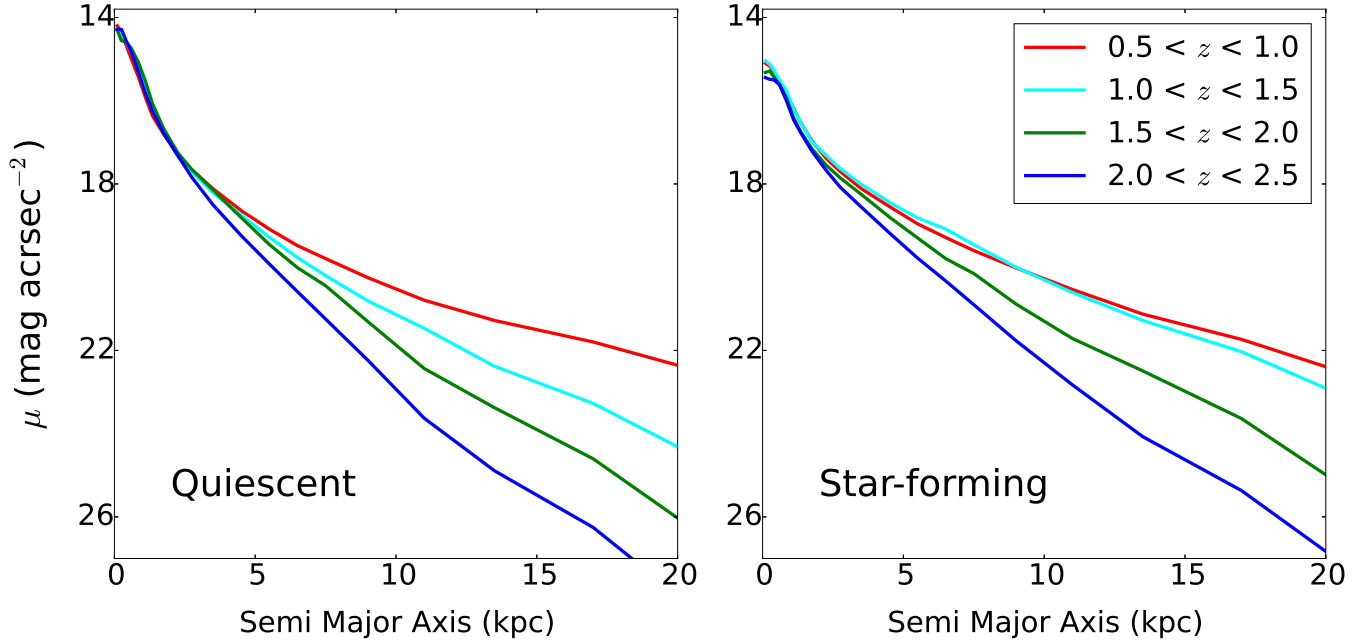


FIG. 11.— The inside-out growth of massive galaxies. Median light distributions of massive quiescent and star-forming galaxies are shown in four redshift bins. While the inner few kpc of these galaxies has been almost intact since $z \approx 2.5$, over time more material is accreted in their outskirts. Accretion onto quiescent galaxies continues at least down to $z \approx 0.5$, while it seems that star-forming galaxies stop accreting by $z \approx 1.0$. The inner region of quiescent galaxies are brighter and have a higher density than the centers of star-forming galaxies.

Thus, from the point of view of one of the main themes of this paper, the clear detection of spiral features in high- z massive galaxies constitutes arguably the strongest, most model-independent evidence for the presence of a substantial disk component in these systems. We see the spiral features only in the star-forming galaxies and not in quiescent systems, but, by analogy with local S0 and spiral galaxies, this is not surprising.

An edge-on view of a galaxy can reveal another indisputable signature of a prominent stellar disk. Figure 10 gives several examples of highly flattened ($e > 0.6$) galaxies in our sample that are consistent with disk structures seen edge-on. Interestingly, most of them are relatively thick. The fraction of galaxies with a stellar disk can be inferred from the frequency of detected edge-on galaxies. For this estimation, we assume a uniform distribution of ellipticity with $0 < e < 0.8$ for a population of bulge+disk systems. The inferred fraction of galaxies with a disk hovers around 40–50% at $1.0 < z < 2.5$, both among star-forming and quiescent galaxies, but below $z = 1$, the incidence of edge-on quiescent galaxies drops to zero (Table 5). Highly flattened systems (especially at high- z) can be hallmarks of merger. However, considering the fact that the majority of these galaxies are compact, the chance of this degeneracy is low.

5. IMPLICATIONS FOR GALAXY EVOLUTION

The discovery of red nuggets has captured much attention in recent years as it requires a new paradigm for the formation and evolution of massive elliptical galaxies. The observed compactness of red nuggets at $z \approx 2$ initially raised the question of whether the massive red galaxies have indeed increased their sizes by a factor of roughly $\sim 3 - 5$ while maintaining their passive state,

or whether the size measurement might in some way be flawed. Extensive recent simulations (Mosleh et al. 2013; Davari et al. 2014, 2016), coupled with consistent results from multiple independent studies (e.g., Daddi et al. 2005; Toft et al. 2007; Trujillo et al. 2007; Buitrago et al. 2008; Cimatti et al. 2008; Franx et al. 2008; van der Wel et al. 2008; van Dokkum et al. 2008; Damjanov et al. 2009; Cassata et al. 2010; Newman et al. 2012; Szomoru et al. 2012), have minimized skepticism on the fidelity of the size measurements.

This work confirms that massive galaxies at $z \approx 2$ were indeed compact, and over the next 10 billion years their sizes have increased significantly (Figure 5). The growth occurred inside-out (Patel et al. 2013; Huang et al. 2013). Figure 11 shows the median light distribution of massive quiescent and star-forming galaxies in four redshift bins. While the inner few kpc of these galaxies have been in place since $z \approx 2.5$, over time more and more material was added to their outskirts. Accretion onto quiescent galaxies continued at least down to $z \approx 0.5$, whereas their star-forming counterparts seem to have stopped growing by $z \approx 1$.

The compactness of the red massive galaxies at higher redshifts and their similarities to SMGs implicate the importance of strong gas dissipation during their early formation epochs, which in turn led to the starburst activity and accompanying disk formation (e.g., Targett et al. 2013; Toft et al. 2014). This raises some important questions: Do red nuggets at $z \approx 2$ have a sizable disk component, and if so, how prevalent was it? And since red nuggets are widely believed to evolve into present-day ellipticals—indeed, our number density selection was specifically chosen to ensure that they do—can we trace

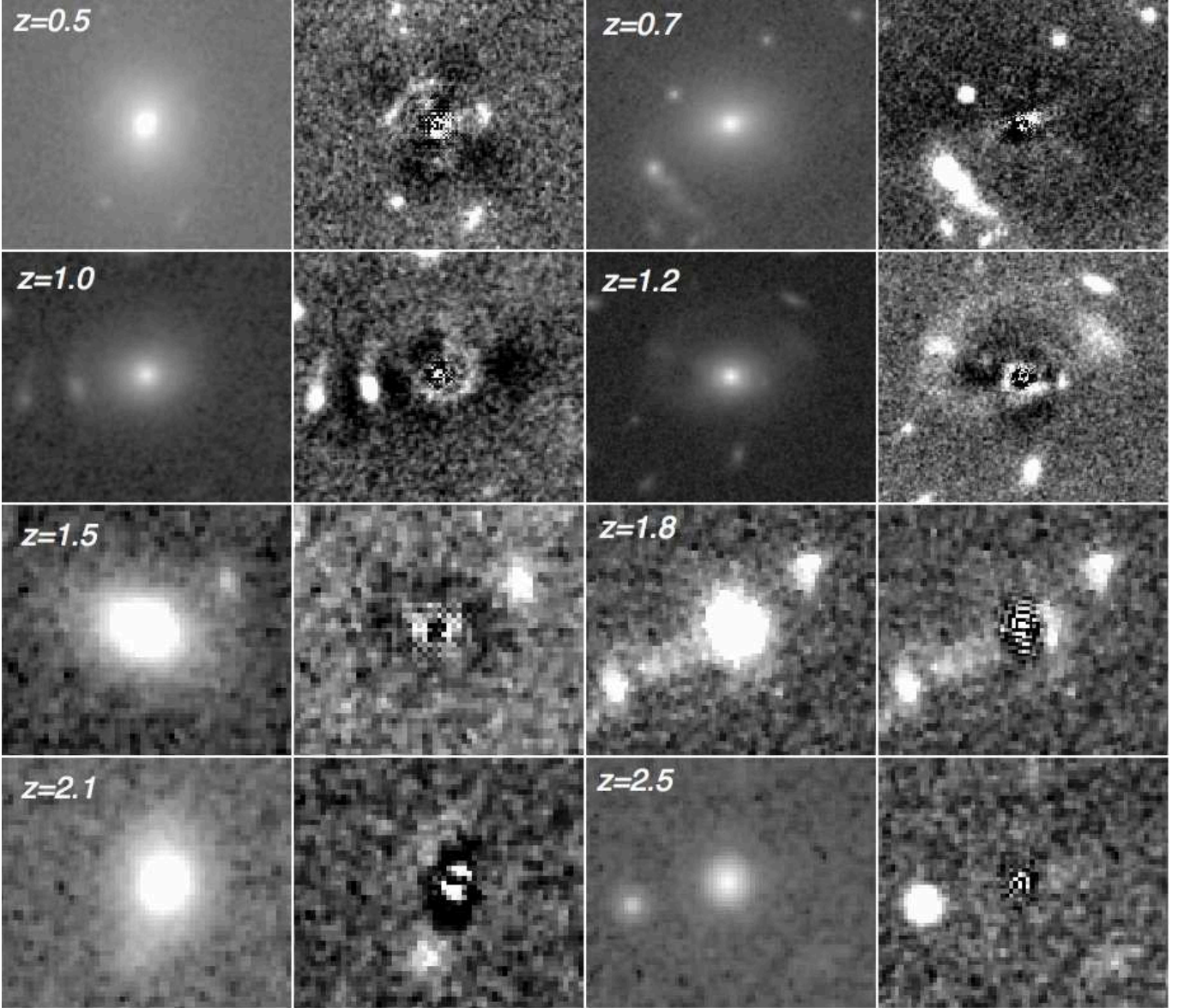


FIG. 12.— Examples of galaxies with tidal features or potentially nearby neighbors, at different redshifts. The residual images, after removal of the bulge+disk model from the original galaxy image, allows for more effective visual detection of non-axisymmetric features.

the redshift evolution of the morphological transformation that must take place?

Table 5 shows the estimated fraction of galaxies with a prominent stellar disk, using three different diagnostics: galaxies with $B/T < 0.5$, visually detectable spiral features (Section 4.3), and inferences from the frequency of detected edge-on ($e > 0.6$; Section 4.3) systems.

Our results suggest that disks may be common among high- z massive galaxies, although it is difficult to obtain a conclusive estimate of their frequency. They range from an absolute minimum of $\sim 5\%$, as deduced from the incidence of spiral arms among star-forming systems, to as high as $\sim 80\%$ for all massive galaxies regardless of star formation activity, according to bulge-disk decomposition. The three disk diagnostics are not equally reliable and informative. While, visually detectable spiral structures are the most reliable indicator of a disk, they provide the lower limit, as the viewing angle and surface brightness dimming can prevent the detection of

these structures. Furthermore, at higher redshifts, disks of massive galaxies may not be favorable to long lived spiral structures. On the other hand, low B/T at higher redshifts does not necessarily mean a disk resides in a galaxy and provides an upper limit. The fitted exponential component is not necessarily an indicator of a disk. Lastly, the inferred fraction of disks using the fraction of edge-on disks is probably the best proxy for the detection of disks.

The prevalence of large-scale disks at $z \approx 2$ is further reinforced by the moderate Sérsic indices and broad distribution of ellipticities derived from the global light distribution, a trend already echoed in other recent investigations. By tracking the population from $z \approx 2.5$ to 0.5 and performing a consistent analysis of the whole sample, we witness the gradual transition of the large-scale morphology. By $z \approx 0.5$, the red massive galaxies attain a high bulge fraction of $B/T \approx 0.8$, signifying the near disappearance of a dominant disk (Figure 6); their global

(Figure 5 and bulge (Figure 7) Sérsic indices converge to $n \approx 4\text{--}5.5$, values close to that of de Vaucouleurs’ profile; and their global axial ratios drop to values closely resembling those of local massive galaxies (e.g., as measured in the GAMA survey). All of these indicators strongly support the thesis that high- z red nuggets are, in fact, the direct ancestors of today’s massive ellipticals.

Much attention has been focused recently on the pivotal role that minor, dry mergers play in the evolution of red nuggets into present-day elliptical galaxies. Minor mergers are considered the most plausible mechanism for explaining the dramatic size growth of massive quiescent galaxies (e.g., Bournaud et al. 2007; Bezanson et al. 2009; Hopkins et al. 2009; Naab et al. 2009; van Dokkum et al. 2010; Oser et al. 2012; Hilz et al. 2013), their mass increase after being quenched (van Dokkum et al. 2010), the multiple-component structure of local ellipticals (Huang et al. 2013a, 2013b), and the prevalence of tidal features seen in deep imaging of nearby massive galaxies (van Dokkum 2005; Tal et al. 2009; Janowiecki et al. 2010).

The simulations of Welker et al. (2015) stress the effectiveness of dry mergers in increasing the sizes of massive compact galaxies. Consistent with Hilz et al. (2013), they find that dry mergers lead to a size-mass relation of the form $R_e \propto M^\gamma$, with $\gamma \approx 2$. This is close to the size evolution we measure, $\alpha = -1.76 \pm 0.16$, for our quiescent massive galaxies between redshift 2.5 and 0.5. Interestingly, star-forming galaxies have a considerably smaller value of $\alpha = -1.17 \pm 0.30$. By $z \approx 1$, more than 80% of the simulated massive galaxies ($M_\star > 10^{10.5} M_\odot$) from Welker et al. (2015) have experienced minor mergers. The merger rate is expected, on average, to increase monotonically with stellar mass (Hopkins et al. (2010)), and therefore should be even higher for our sample. Figure 12 shows a number of galaxies from our sample with disturbed morphologies and small-scale structure that may be indicative of merging activity. We estimate, from visual inspection, that at $0.5 < z < 1.0$ more than 60% of quiescent galaxies have small nearby objects or show merger signatures (e.g., distortions, tidal tails, and shells); about 40% of star-forming galaxies show similar features. By $1.0 < z < 1.5$, the fraction of merger candidates, for both classes combined, drops to $\sim 30\%$, presumably because it becomes increasingly difficult to resolve small-scale structure for distant galaxies. While these morphological indicators are by no means secure estimators of the merger fraction, they at least give the qualitative impression that mergers—especially minor mergers—play a part in the morphological transformation of massive galaxies.

The discovery of a significant disk component in massive galaxies at $z \approx 2$ and their eventual disappearance toward lower redshifts brings an important new element to the story. How were the disks destroyed? Can this be accomplished by minor mergers alone? Most likely not. Breaking a big disk requires hitting it with something hefty, which can only be accomplished with a major merger. The simulations of Hopkins et al. (2010) show that major mergers are needed for forming galaxies with high B/T .

Another key player in the evolutionary scenario of massive galaxies is, one that has captured less attention, are the compact blue galaxies. Although star-forming galaxies

are larger than quiescent galaxies at each redshift bin, at high redshifts these galaxies are compact, as well (Figure 5). As local star-forming massive galaxies are rare (e.g., Baldry et al. 2012), most of high-redshift compact blue galaxies must have also evolved into present-day massive ellipticals. Figure 2 illustrates how over time the star-forming massive galaxies turn into quiescent massive galaxies. At the same time that the blue population quenches star formation, significant morphological transformation must also occur to elevate the relative bulge fraction (Figure 6) and increase the Sérsic index (both globally and for the bulge alone; Figure 5 and 7).

The prevalence of prominent stellar disks at higher redshifts raises the possibility that some of these bulge+disk massive galaxies may have survived to the present. Where are they? The “superluminous” spiral galaxies discussed by Ogle et al. (2016) seem to fit the description. Ogle et al. quote an average number density of 32 Gpc^{-3} at $z < 0.3$. Interestingly, the fraction of star-forming massive galaxies with spiral arms is 30% at $z \approx 0.5$ (Table 5). As our overall sample was chosen to satisfy $n_c = 1.4 \times 10^{-4} \text{ Mpc}^{-3}$, the observed number density of massive spirals in our lowest redshift bin is $0.3n_c$, or 42 Gpc^{-3} , very close to the average number density given by Ogle et al. 2015. (We note, however, that the sample size of star-forming massive galaxies at the lowest redshift bin is not statistically significant, as discussed in Section 4.3.) Wellons et al. (2015), using the Illustris (Vogelsberger et al. 2014; Genel et al. 2014) cosmological hydrodynamical simulations, trace the evolution of 35 massive compact galaxies from $z = 2$. They find that $\sim 30\%$ of their galaxies survive undisturbed, while the rest have either experienced inside-out growth or have been destroyed via major mergers.

6. SUMMARY

The discovery of massive compact galaxies at high redshift, specially red nuggets, has offered new insights into galaxy formation and evolution. These massive galaxies have major differences with their local counterparts, the massive ellipticals. They are not only compact but, as demonstrated in this study, they also possess a stellar disk. To match the population of present-day ellipticals, red nuggets must increase significantly in size and destroy their disks. Using a homogeneous and unbiased sample of ~ 250 massive galaxies in the CANDELS fields, spanning the redshift range $0.5 < z < 2.5$, and selected through the fixed number density technique, we studied the evolution of morphological parameters as a function of redshift. Further, we classified galaxies into quiescent and star-forming systems using the UVJ color-color diagram in order to trace separately their evolutionary histories.

We conclude:

- The fraction of quiescent massive galaxies is higher at lower redshifts.
- Both star-forming and quiescent galaxies have increased their sizes significantly from $z \approx 2.5$ to the present time, and the growth has occurred inside-out.
- The global Sérsic index of quiescent galaxies has increased over time (from $n \approx 2.5$ to $n > 4$), while

that of star-forming galaxies has remained roughly constant ($n \approx 2.5$).

- The distribution of global ellipticities has changed mildly with time, becoming rounder toward lower redshifts.
- The typical value of B/T has increased with decreasing redshift, both for the quiescent and star-forming subsamples. By $z \approx 0.5$, massive quiescent galaxies (with $B/T \approx 0.8$) begin to resemble the local elliptical galaxies. Star-forming galaxies have a lower median B/T at each redshift bin.
- The evolution of Sérsic index, ellipticity, and B/T suggests that both star-forming and quiescent galaxies have a significant stellar disk at early times, which systematically became less prominent toward lower redshifts.
- A considerable fraction of our sample have visually detectable spiral structures or thin disks observed

nearly edge-on, which further confirms that high- z massive galaxies have prominent stellar disks.

- While minor dry mergers can explain the inside-out growth of massive galaxies, major mergers are needed to destroy their stellar disks between redshift 2.5 and the present time.
- While the disks of star-forming and quiescent galaxies evolve similarly, their bulges follow different evolutionary trajectories. The size increase of the bulges of quiescent galaxies is more significant and their Sérsic indices and axial ratios are, on average, higher than their star-forming counterparts.

RD has been funded by a graduate student fellowship awarded by Carnegie Observatories. LCH acknowledges support by the Chinese Academy of Science through grant No. XDB09030102 (Emergence of Cosmological Structures) from the Strategic Priority Research Program and by the National Natural Science Foundation of China through grant No. 11473002. RD thanks Heather Worthington-Davari for providing long-term support.

REFERENCES

- Baldry, I. K., Driver, S. P., Loveday, J., et al. 2012, *MNRAS*, 421, 621
- Barnes, J. E., & Hernquist, L. 1992, *ARA&A*, 30, 705
- Bezanson, R., van Dokkum, P. G., Tal, T., et al. 2009, *ApJ*, 697, 1290
- Blanton, M. R., Hogg, D. W., Bahcall, N. A., et al. 2003, *ApJ*, 592, 819
- Bournaud, F., & Elmegreen, B. G. 2009, *ApJ*, 694, L158
- Bournaud, F., Elmegreen, B. G., & Elmegreen, D. M. 2007, *ApJ*, 670, 237
- Brammer, G. B., van Dokkum, P. G., & Coppi, P. 2008, *ApJ*, 686, 1503
- Brammer, G. B., Whitaker, K. E., van Dokkum, P. G., et al. 2011, *ApJ*, 739, 24
- Bruce, V. A., Dunlop, J. S., Cirasuolo, M., et al. 2012, *MNRAS*, 427, 1666
- Bruce, V. A., Dunlop, J. S., McLure, R. J., et al. 2014, *MNRAS*, 444, 1001
- Bruce, V. A., Dunlop, J. S., McLure, R. J., et al. 2014, *MNRAS*, 444, 1660
- Buitrago, F., Trujillo, I., Conselice, C. J., et al. 2008, *ApJ*, 687, L61
- Cassata, P., Giavalisco, M., Guo, Y., et al. 2010, *ApJ*, 714, L79
- Cassata, P., Giavalisco, M., Guo, Y., et al. 2011, *ApJ*, 743, 96
- Chang, Y.-Y., van der Wel, A., Rix, H.-W., et al. 2013, *ApJ*, 762, 83
- Cimatti, A., Cassata, P., Pozzetti, L., et al. 2008, *A&A*, 482, 21
- Ciotti, L. 1991, *A&A*, 249, 99
- Conselice, C. J., Blackburne, J. A., & Papovich, C. 2005, *ApJ*, 620, 564
- Conselice, C. J., Bluck, A. F. L., Ravindranath, S., et al. 2011, *MNRAS*, 417, 2770
- Daddi, E., Renzini, A., Pirzkal, N., et al. 2005, *ApJ*, 626, 680
- Dahlen, T., Mobasher, B., Faber, S. M., et al. 2013, *ApJ*, 775, 93
- Damjanov, I., McCarthy, P. J., Abraham, R. G., et al. 2009, *ApJ*, 695, 101
- Davari, R., Ho, L. C., Peng, C. Y., & Huang, S. 2014, *ApJ*, 787, 69
- Davari, R., Ho, L. C., & Peng, C. Y. 2016, *ApJ*, 824, 112
- Davis, M., Guhathakurta, P., Konidaris, N. P., et al. 2007, *ApJ*, 660, L1
- de Vaucouleurs, G. 1948, *Annales d'Astrophysique*, 11, 247
- Dobbs, C., & Baba, J. 2014, *PASA*, 31, 35
- Driver, S. P., GAMA Team, Baldry, I. K., et al. 2009, in *IAU Symposium*, Vol. 254, IAU Symposium, ed. J. Andersen, Nordströara, B. m, & J. Bland-Hawthorn, 469–474
- Elmegreen, D. M., & Elmegreen, B. G. 2014, *ApJ*, 781, 11
- Fathi, K., & Peletier, R. F. 2003, *A&A*, 407, 61
- Fisher, D. B., & Drory, N. 2008, *AJ*, 136, 773
- Franx, M., van Dokkum, P. G., Schreiber, N. M. F., et al. 2008, *ApJ*, 688, 770
- Freeman, K. C. 1970, *ApJ*, 160, 811
- Genel, S., Vogelsberger, M., Springel, V., et al. 2014, *MNRAS*, 445, 175
- Genzel, R., Tacconi, L. J., Eisenhauer, F., et al. 2006, *Nature*, 442, 786
- Giavalisco, M., Ferguson, H. C., Koekemoer, A. M., et al. 2004, *ApJ*, 600, L93
- Graham, A. W., & Worley, C. C. 2008, *MNRAS*, 388, 1708
- Grogin, N. A., Kocevski, D. D., Faber, S. M., et al. 2011, *ApJS*, 197, 35
- Hilz, M., Naab, T., & Ostriker, J. P. 2013, *MNRAS*, 429, 2924
- Hopkins, P. F., Bundy, K., Croton, D., et al. 2010, *ApJ*, 715, 202
- Hopkins, P. F., Bundy, K., Murray, N., et al. 2009, *MNRAS*, 398, 898
- Huang, S., Ho, L. C., Peng, C. Y., Li, Z.-Y., & Barth, A. J. 2013, *ApJ*, 768, L28
- Ichikawa, T., Kajisawa, M., & Akhlaghi, M. 2012, *MNRAS*, 422, 1014
- Janowiecki, S., Mihos, J. C., Harding, P., et al. 2010, *ApJ*, 715, 972
- Jedrzejewski, R. I. 1987, *MNRAS*, 226, 747
- Koekemoer, A. M., Faber, S. M., Ferguson, H. C., et al. 2011, *ApJS*, 197, 36
- Kovács, A., Chapman, S. C., Dowell, C. D., et al. 2006, *ApJ*, 650, 592
- Krist, J. E., Hook, R. N., & Stoehr, F. 2011, *SPIE*, 8127
- Labbé, I., Bouwens, R., Illingworth, G. D., & Franx, M. 2006, *ApJ*, 649, L67
- Lang, P., Wuyts, S., Somerville, R. S., et al. 2014, *ApJ*, 788, 11
- Law, D. R., Steidel, C. C., Erb, D. K., et al. 2007, *ApJ*, 669, 929
- Law, D. R., Steidel, C. C., Erb, D. K., et al. 2009, *ApJ*, 697, 2057
- Lawrence, A., Warren, S. J., Almaini, O., et al. 2007, *MNRAS*, 379, 1599
- Leja, J., van Dokkum, P., & Franx, M. 2013, *ApJ*, 766, 33
- Lemson, G., & Virgo Consortium, t. 2006, *ArXiv Astrophysics e-prints*, astro-ph/0608019
- Lintott, C., Schawinski, K., Bamford, S., et al. 2011, *MNRAS*, 410, 166
- Liske, J., Baldry, I. K., Driver, S. P., et al. 2015, *MNRAS*, 452, 2087
- Magnelli, B., Lutz, D., Berta, S., et al. 2010a, *A&A*, 518, L28
- Mancini, C., Daddi, E., Renzini, A., et al. 2010, *MNRAS*, 401, 933
- Michałowski, M. J., Dunlop, J. S., Cirasuolo, M., et al. 2012, *A&A*, 541, A85
- Mobasher, B., Dahlen, T., Ferguson, H. C., et al. 2015, *ApJ*, 808, 101
- Morishita, T., Ichikawa, T., & Kajisawa, M. 2014, *ApJ*, 785, 18
- Mosleh, M., Williams, R. J., & Franx, M. 2013, *ApJ*, 777, 117
- Mundy, C. J., Conselice, C. J., & Ownsworth, J. R. 2015, *MNRAS*, 450, 3696

- Muzzin, A., Marchesini, D., Stefanon, M., et al. 2013, *ApJS*, 206, 8
- Naab, T., Johansson, P. H., & Ostriker, J. P. 2009, *ApJ*, 699, L178
- Naab, T., Johansson, P. H., Ostriker, J. P., & Efstathiou, G. 2007, *ApJ*, 658, 710
- Newman, A. B., Ellis, R. S., Bundy, K., & Treu, T. 2012, *ApJ*, 746, 162
- Ogle, P. M., Lanz, L., Nader, C., & Helou, G. 2015, *arXiv:1511.00659*
- Oser, L., Naab, T., Ostriker, J. P., & Johansson, P. H. 2012, *ApJ*, 744, 63
- Papovich, C., Finkelstein, S. L., Ferguson, H. C., Lotz, J. M., & Giavalisco, M. 2011, *MNRAS*, 412, 1123
- Patel, S. G., van Dokkum, P. G., Franx, M., et al. 2013, *ApJ*, 766, 15
- Peng, C. Y., Ho, L. C., Impey, C. D., & Rix, H.-W. 2010, *AJ*, 139, 2097
- Poggianti, B. M., Calvi, R., Bindoni, D., et al. 2013, *ApJ*, 762, 77
- Robertson, B., Bullock, J. S., Cox, T. J., et al. 2006, *ApJ*, 645, 986
- Santini, P., Ferguson, H. C., Fontana, A., et al. 2015, *ApJ*, 801, 97
- Saracco, P., Longhetti, M., & Gargiulo, A. 2010, *MNRAS*, 408, L21
- Schulz, J., Fritze-v. Alvensleben, U., & Fricke, K. J. 2003, *A&A*, 398, 89
- Scoville, N., Abraham, R. G., Aussel, H., et al. 2007a, *ApJS*, 172, 38
- Scoville, N., Aussel, H., Brusa, M., et al. 2007b, *ApJS*, 172, 1
- Skelton, R. E., Whitaker, K. E., Momcheva, I. G., et al. 2014, *ApJS*, 214, 24
- Springel, V., & Hernquist, L. 2005, *ApJ*, 622, L9
- Springel, V., White, S. D. M., Jenkins, A., et al. 2005, *Nature*, 435, 629
- Szomoru, D., Franx, M., Bouwens, R. J., et al. 2011, *ApJ*, 735, L22
- Szomoru, D., Franx, M., & van Dokkum, P. G. 2012, *ApJ*, 749, 121
- Tal, T., van Dokkum, P. G., Nelan, J., & Bezanson, R. 2009, *AJ*, 138, 1417
- Targett, T. A., Dunlop, J. S., Cirasuolo, M., et al. 2013, *MNRAS*, 432, 2012
- Taylor, E. N., Franx, M., Glazebrook, K., et al. 2010, *ApJ*, 720, 723
- Thomas, D., Maraston, C., Bender, R., & Mendes de Oliveira, C. 2005, *ApJ*, 621, 673
- Toft, S., Smolčić, V., Magnelli, B., et al. 2014, *ApJ*, 782, 68
- Toft, S., van Dokkum, P., Franx, M., et al. 2007, *ApJ*, 671, 285
- Toomre, A. 1977, *ARA&A*, 15, 437
- Trujillo, I., Cenarro, A. J., de Lorenzo-Cáceres, A., et al. 2009, *ApJ*, 692, L118
- Trujillo, I., Conselice, C. J., Bundy, K., et al. 2007, *MNRAS*, 382, 109
- Valentinuzzi, T., Fritz, J., Poggianti, B. M., et al. 2010, *ApJ*, 712, 226
- van der Wel, A., Bell, E. F., Häussler, B., et al. 2012, *ApJS*, 203, 24
- van der Wel, A., Holden, B. P., Zirm, A. W., et al. 2008, *ApJ*, 688, 48
- van der Wel, A., Rix, H.-W., Holden, B. P., Bell, E. F., & Robaina, A. R. 2009, *ApJ*, 706, L120
- van Dokkum, P. G. 2005, *AJ*, 130, 2647
- van Dokkum, P. G., Franx, M., Kriek, M., et al. 2008, *ApJ*, 677, L5
- van Dokkum, P. G., Whitaker, K. E., Brammer, G., et al. 2010, *ApJ*, 709, 1018
- Vogelsberger, M., Genel, S., Springel, V., et al. 2014, *MNRAS*, 444, 1518
- Welker, C., Dubois, Y., Devriendt, J., et al. 2015, *ArXiv e-prints*, *arXiv:1502.05053*
- Wellons, S., Torrey, P., Ma, C.-P., et al. 2015, *MNRAS*, 449, 361
- Whitaker, K. E., Labbé, I., van Dokkum, P. G., et al. 2011, *ApJ*, 735, 86
- Willett, K. W., Lintott, C. J., Bamford, S. P., et al. 2013, *MNRAS*, 435, 2835
- Williams, C. C., Giavalisco, M., Cassata, P., et al. 2014, *ApJ*, 780, 1
- Williams, R. J., Quadri, R. F., Franx, M., van Dokkum, P., & Labbé, I. 2009, *ApJ*, 691, 1879
- Wirth, A. 1981, *AJ*, 86, 981
- Wuyts, S., Labbé, I., Franx, M., et al. 2007, *ApJ*, 655, 51
- Zirm, A. W., van der Wel, A., Franx, M., et al. 2007, *ApJ*, 656, 66